J Mater Sci (2009) 44:483–491
DOI 10.1007/s10853-008-3099-7

Measurement and modelling of heat transfer in paper coating structures

Philip Gerstner · Jouni Paltakari · Patrick A. C. Gane

Received: 13 August 2008 / Accepted: 30 October 2008 / Published online: 23 November 2008

Abstract Thermal conductivity of paper coatings is increasingly important in the performance of many printing processes, including traditional heatset web offset and thermal papers, as well as digital processes, such as electrophotography. This work studies the extension of a Modified Lumped Parameter Model, previously used successfully to describe talc coatings, to model the thermal conductivity–coating structure relationships of calcium carbonate (gcc: 60 wt% < 2 μm) coatings. A series of compact tablets were used to provide experimental values of thermal diffusivity and conductivity. The samples studied covered a range of latex binder addition levels, namely 0–25 parts, based on 100 parts pigment, of 0.2 μm styrene acrylate latex. Combining the observed thermal properties with knowledge of the pore structure changes induced by the latex addition, it is possible to establish initial correlation with the model, in which the connectivity of the structure is increased at low latex dose illustrating the initial increase in effective thermal conductivity. The practically hard sphere properties of the latex used, combined with the broad size distribution of the gcc, produce a disruptive packing effect as the dose level increases, such that the conductivity reflects a competition between the increasing connectivity provided by the latex versus the increasing relative pore size in the network structure. It is recognized that the fixed pigment volume in the model unit cell diverts from a true representation of the residual porosity. At the highest latex dose levels, the intrinsically less conducting properties of the latex begin to dominate.

P. Gerstner (✉) · J. Paltakari · P. A. C. Gane
Department of Forest Products Technology, Faculty of Chemistry and Materials Science, Helsinki University of Technology, Vuorimiehentie 1A, P.O. Box 6300, 02150 Espoo, Finland
e-mail: Philip.Gerstner@tkk.fi

P. A. C. Gane
Omya Development AG, 4665 Oftringen, Switzerland

Introduction

Heat transfer through paper coatings plays an important role in many fields of coated paper production, conversion or printing. Most evident are processes such as drying of coatings, thermal calendering as well as offset and electrophotographic printing. But also in emerging technologies such as in dry surface treatment, a process in which binder covered pigment is fused thermally onto the paper surface, heat transfer through the coating structure is significant [1]. In order to improve those processes from both an economical point of view (in terms of energy efficiency) and from the perspective of product quality, knowledge of the thermal properties is required. The thermal properties and heat transfer in paper have been studied over the past decades [2–4]. However, limited attention has been paid to the thermal behaviour of paper coatings. With the increasing use of coated high-quality printing papers [5], there is a need in printing technology for the thermal properties of paper coatings to be understood. The coating layer is the receiving interface in printing processes. This study highlights the importance of the mechanisms for thermal conductivity of paper coatings in order to be able to design coatings for optimal thermal efficiencies in printing and other heat applying processes.

As the thermal properties alone are not used to define the recipe of a coating colour, it is important to understand the effect of different coating structures and formulation components on the resulting thermal properties. Tsotsas

and Martin [6] classified primary effects such as the thermal conductivities of the individual phases, or the role of porosity, and secondary effects like thermal conductivity by area contact or particle shape and size distributions. The work here studies the potential of developing a model to describe the generic thermal behaviour of coatings, namely the thermal conductivity k (see Eq. 1) as a function of structural and material properties,

$$k = D\rho c_p \quad (1)$$

where thermal diffusivity D is measured experimentally by the temperature response of a one side heated pigment-containing tablet, a method that has been adapted from a previous study by Gane et al. [7]. The effective heat capacity c_p (at constant pressure) is calculated for the material components and together with the measured tablet density, ρ, the thermal conductivity k can be calculated. To get information about the structure, total porosity and pore size distribution is measured using mercury porosimetry. This enables the use of structural models to examine the role of the network of skeletal (solid) material making up the porous structure in determining the thermal conductivity of coating structures.

In general, modelling of heat transfer in porous media has been developed over the last century. In his work on magnetism, Maxwell [8] pointed out the similarities of electrical and thermal conduction. Later, more abstract models using the parallels of electrical and thermal conductance were developed. Gerstner et al. [9] modified the lumped parameter model by Hsu et al. [10] for the needs of paper coatings and showed that using a binder dosage variable and a pigment content variable was more favourable compared to applying porosity alone. This model, combined with porosity as an additional parameter, will be used in this paper to discuss the interconnection of structural and thermal properties of a calcium carbonate coating structure.

Experimental

Materials

The pigment used in all the experiments was an industry standard ground calcium carbonate (gcc), Hydrocarb 60.[1] The pigment comes in polyacrylate-dispersed slurry form having a solids content of 78 wt%. The binder used was the *n*-butyl acrylate styrene latex Acronal S360D.[2] The basic properties of pigment and binder are given in Tables 1 and 2, respectively. Coating colour mixtures were prepared using binder-free slurry in both the original dispersed form and when charge flocculated, as well as dispersed coating slurry with binder concentrations of 8, 12, 20 and 25 wt% based on pigment. The flocculant used was Catiofast CS[3] in a concentration of 1 wt% based on pigment.

Table 1 Basic properties of the gcc pigment used in the experiments

	gcc
$CaCO_3$ content	98%
Parts <2 μm	60 wt%
Slurry solids content	78 wt%
Slurry density	1965 kg m^{-3}
pH	9
Viscosity	500 mPa·s

Table 2 Basic properties of the SA latex used in the experiments

	SA latex
MFFT[a]	<1 °C
Average particle size	0.2 μm
Solids content	50 wt%
Density	1050 kg m^{-3}
pH	8
Viscosity	375 mPa·s

[a] Minimum film forming temperature

Tablet forming

The tablets were formed in a pressure vessel, as shown in Fig. 1. A constantly applied pressure of p = 20 bar dewaters the slurry through a membrane which is supported by a screen and sealed by rubber rings. The membrane has a mesh size of d = 0.025 μm, which is small compared to the average latex particle size of ca. 0.2 μm. For all tablets, approximately 50 cm^3 of slurry was used (ca. 2/3 of the vessel's volume) in order to maintain a constant dewatering time and tablet thickness. The dewatering time depends strongly on latex content. The times, as given in Table 3, were set so that after the tablet forming there is still liquid slurry left on top of the tablet. The liquid is decanted before the tablet is removed. This is to avoid air from being pressed through the tablet structure, which might change binder distribution or isotropy of the tablet structure. It also improves evenness and smoothness of the tablet's top surface.

After forming and decanting of the remaining slurry, the tablets were removed by a metal stamp pressing the tablets from the membrane side out of the hollow forming cylinder. The tablets were then oven dried at 60 °C. During the drying a slight deformation of the tablets could be

[1] Hydrocarb 60 is a registered trademark of Omya AG.

[2] Acronal S360D is a registered trademark of the BASF AG.

[3] Catiofast CS is a registered trademark of the BASF AG.

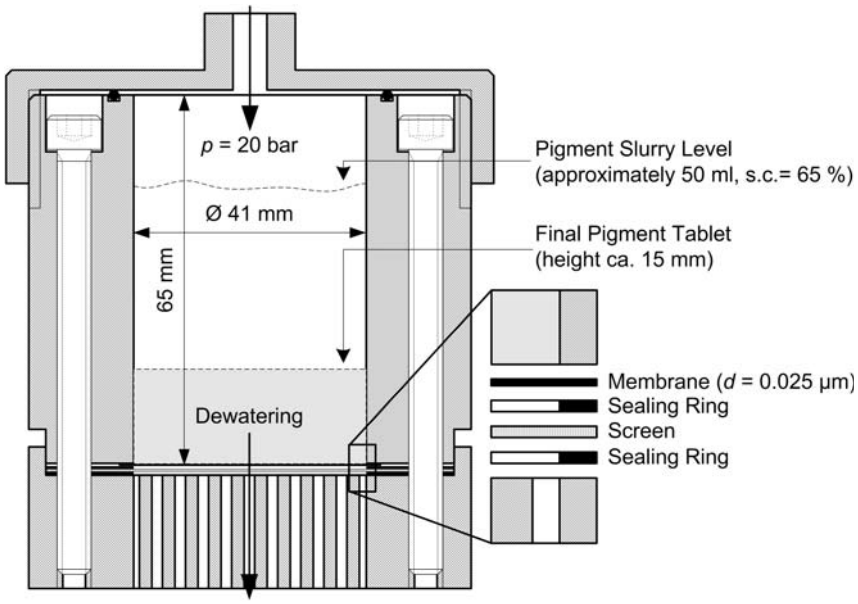

Fig. 1 Tablet forming by dewatering of the coating slurry through a membrane

Table 3 Forming times for tablets of different slurries

Latex (wt%)	Forming time
0	40 min
0	40 min[a]
8	100 min
12	180 min
20	24 h
25	>24 h[b]

[a] Flocculated slurry, extended forming time due to difficulties to remove liquid slurry

[b] Forming incomplete

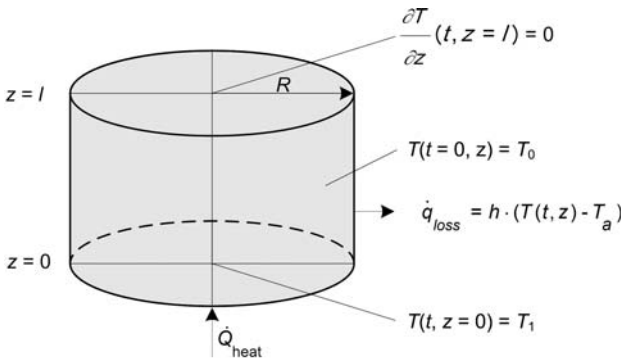

Fig. 2 Theoretical experimental layout for heat conduction along the axis of a cylinder, including the initial and boundary conditions as well as heat losses

observed. Higher binder content resulted in a higher shrinkage. Tablets of 20 and 25 parts binder even showed small cracks at the surface due to the high shrinkage. In order to get a well-defined cylindrical tablet shape and in order to remove surface cracks, all the tablets were ground after drying, using a rotational grinder running at 200 rpm equipped with coarse grinding paper (P240) for the first rough shaping. Subsequently, fine grinding was done manually using P600 grinding paper. The tablets were ground to thicknesses of approximately 14 mm. Their diameter varies from 38 to 40 mm depending on the forming quality. For the calculations their individual dimensions were used.

Thermal diffusivity measurement

The heat transfer through a tablet can be described as the heat conduction along the axis of a cylinder (see Fig. 2). For the experiment, it can be assumed, because of the uniform heat source, that the heat flux through the tablet is homogeneous in the z direction. Because the radius (R) of the tablet is large compared to its thickness (l), and the tablet is insulated in the radial direction, the temperature gradient in the radial direction reduces to zero and the heat diffusion equation reduces to its one-dimensional transient form. Since the tablet is insulated in the radial direction and on top, the heat losses due to external convection would ideally become zero. Since this case cannot be reached in practice, the heat losses need to be taken into account. For a thermal conductivity independent of z position and temperature, the heat diffusion equation becomes:

$$k\frac{\partial^2 T}{\partial z^2} - \dot{q}_{\text{loss}} = \rho c_{\text{p}}\frac{\partial T}{\partial t} \tag{2a}$$

$$D\frac{\partial^2 T}{\partial z^2} - \frac{\partial T}{\partial t} = h(T - T_{\text{a}}) \tag{2b}$$

where k is the thermal conductivity (W m^{-1} K^{-1}), T the temperature (°C), z the tablet thickness coordinate (m), $\dot{q}_{\text{loss}}$

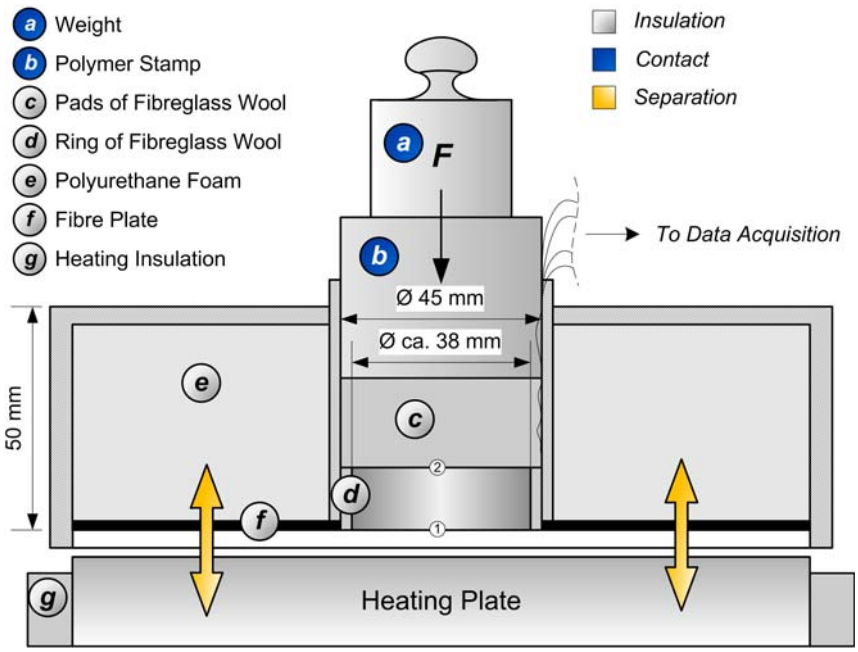

Fig. 3 Setup for the measurement of thermal diffusivity

describes the heat losses (W m^{-2} s^{-1}), ρ the density (kg m^{-3}), c_p the heat capacity (J kg^{-1} K^{-1}), t the time (s) and D is the thermal diffusivity (m^2 s^{-1}).

The tablets were acclimatised to $T_1 = 23$ °C at least 12 h before the experiment. Therefore, the initial condition is that the material has an even temperature T_1 throughout its thickness (l):

$$T(z, t = 0) = T_1 \quad 0 \leq z \leq l \tag{3}$$

A two-point controller regulates the temperature of the heating plate at the bottom of the tablet and keeps it within a certain interval. Ideally, the temperature of the heated side is constant during the experimental time, in this case at $T_2 = 100$ °C. The boundary condition at $z = 0$ for the total experimental time τ given by the Dirichlet boundary condition:

$$T(z = 0, t) = T_2 \quad 0 < t \leq \tau \tag{4}$$

The topside of the tablet is insulated, thus no heat flux from the top occurs. This is the Neumann boundary condition:

$$\frac{\partial T}{\partial z}(z = l, t) = 0 \quad 0 \leq t \leq \tau \tag{5}$$

The initial condition (Eq. 3) and the boundary conditions (Eqs. 4 and 5) are used to define the partial differential equation (2b).

In order to meet the previously discussed boundary conditions in practice, the tablets need to be thermally insulated on top and around the shell. At the bottom they need to be in close contact with the heat source. In addition, it is necessary to keep the insulated tablet separate from the heat source until it has reached its target temperature. In order to fulfil those demands, an insulating case was constructed. Figure 3 shows the heating plate together with the insulating case pointing out its three main tasks.

To ensure close contact with the heating surface, a flat stainless steel heating plate was used as a heat source. Its surface was polished at the contact area before the experiments. The heating plate itself was insulated (Fig. 3g) in order to keep the temperature constant for a longer time. The temperature of the heating plate should be constant during the experimental time and uniform at the tablet contact area. The temperature was measured by a thermocouple positioned in a drill hole in the heating plate. This measured temperature triggered a relay for the power supply of the heating plate.

The tablet was surrounded by a ring of fibreglass wool (Fig. 3d) and thus it was held loosely at the bottom of the insulation case. This ring is for radial insulation, but also to compensate for different tablet diameters. As described earlier, the tablet diameters vary due to their different forming quality. The fibreglass ring had to be replaced for every new measurement. On top of the tablet there was fibreglass wool for axial insulation (Fig. 3c). When the case is brought into contact with the heating plate, a weight and a stamp presses the tablet towards the heating plate (Fig. 3a, b). The weight used for all measurements had a mass of 7 kg. For all measurements there was at least one thermocouple at the bottom (number 1 in Fig. 3)

and one at the top of the tablet (number 2 in Fig. 3) to measure the actual heating temperature and the temperature response. In further discussions, the temperature measurements will be numbered from bottom to top in ascending order.

When the tablet had been mounted in the insulating case, the thermocouples were connected via an extension cable to the interface of the data acquisition system. As soon as the temperature of the heating plate reached its target temperature, the temperature recording was started and the insulation case had been placed on top of the heating plate. Finally, the weight was put on top to ensure close contact. For all the measurements, the data were recorded with a sampling rate of $f_s = 10$ Hz. The total experimental time ranged between $\tau = 1200$–1400 s. Because of the two-point control of the heating plate, and the slow reaction time of the entire thermal system, the temperature at the contact area varied slightly. However, it was possible to keep the variation of the heating temperature small. The mean standard deviation of the heating temperatures for the measurements was 1.25 °C.

The thermal diffusivity was then calculated by matching the numerical solution of the heat diffusion equation (Eq. 2b) to the measured topside temperature response. This is done by a self-adaptive iteration of the parameters thermal diffusivity and heat loss. The numerical solution matching the experimental curve delivered the value for thermal diffusivity.

Heat capacity

The effective heat capacity of the sample material (c_{eff}) is calculated additively for the mass share of the two phases of pigment (c_{s1}) and binder (c_{s2}):

$$m_{\text{tot}} c_{\text{eff}} = m_{s1} c_{s1} + m_{s2} c_{s2} \tag{6a}$$

The contribution of air in pores to the total heat capacity is neglected because of its very low mass and low specific heat capacity compared to the solid phases. With $m_{\text{tot}} = m_{s1} + m_{s2}$ and $m_{s2} = \beta m_{s1}$, the effective heat capacity becomes:

$$c_{\text{eff}} = \frac{c_{s1} + \beta c_{s2}}{1 + \beta} \tag{6b}$$

where β is the binder dosage in wt% with respect to 100 wt% pigment. For the individual phases, literature values of $c_{s1} = 880$ J kg^{-1} K^{-1} [11] and $c_{s2} = 559.8$ J kg^{-1} K^{-1} [12] are used for calcium carbonate (pigment) and *n*-butyl acrylate (binder), respectively. Table 4 shows the calculated heat capacities for the tablets. Although no literature values of a styrene acrylate copolymer could be found, the heat capacity of polystyrene itself is listed as

Table 4 Calculated heat capacities for tablets of different binder dosages

Binder (wt%)	Heat capacity (J kg^{-1} K^{-1})
0	880.00
8	856.28
12	845.69
20	826.63
25	815.96

$c_{\text{styrene}} = 454.8$ J kg^{-1} K^{-1} [12]. This value is lower than the one for *n*-butyl acrylate, but it shows that even in the extreme case of using the lowest value for c_{s2}, the calculated effective heat capacity of the tablets containing 25 wt% binder would only be less than 2.6% lower. For the following discussion this possible difference is insignificant.

Porosimetry

A portion of each tablet block is characterised by mercury porosimetry for both porosity and pore size distribution using a Micromeritics Autopore IV mercury porosimeter. The maximum applied pressure of mercury was 414 MPa, equivalent to a Laplace throat diameter of 0.004 μm. The mercury intrusion measurements were corrected for the compression of mercury, expansion of the penetrometer and, where appropriate, the compression of the solid phase of the sample using the equation of Gane et al. [13].

Modelling

The Modified Lumped Parameter Model consists of a unit cell (Fig. 4) and is based on the lumped parameter model introduced by Hsu et al. [10]. Its effective thermal conductivity is calculated by splitting up the unit cell into an arrangement of serial and parallel thermal resistors. The unit cell consists of a square solid phase k_{s1} that represents the pigment. Its size is controlled by the pigment variable a. Placed as a proportion of material contact with the pigment is a second solid phase k_{s2}, representing the binder. The width of the "binder bridges" is defined by the binder variable c. The rest of the unit cell is filled with air k_f.

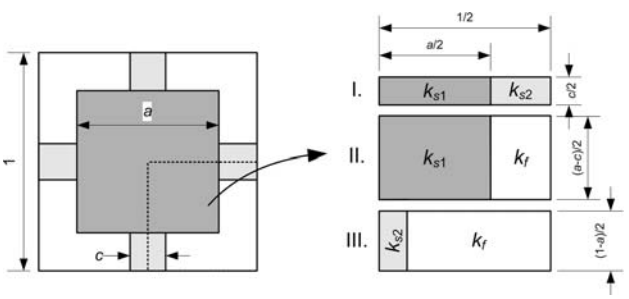

Fig. 4 Unit cell of the modified lumped parameter model [9]

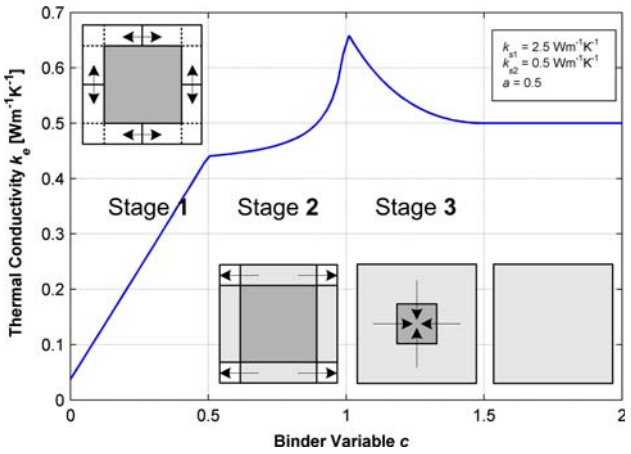

Fig. 5 Three stages of the Modified Lumped Parameter Model. In stage one, binder bridges form. In stage two, porosity goes to zero as it is filled with binder, and in stage three the share of binder to pigment increases further [9]

The model distinguishes between three stages of binder dosage, which are expressed by the binder variable c (Fig. 5). In stage one, binder bridges form around the pigment until the binder bridges equal the size of the pigment. In stage two, the remaining void spaces are filled, before in stage three the share of binder to pigment increases. Gerstner et al. [9] showed that it is possible to model the effective thermal conductivity of a talcum pigment coating which was measured by Guérin et al. [14] by the use of literature values for the materials and a quadratic relation of binder dosage and the model binder variable.

Results and discussion

Thermal properties

In Fig. 6, the effect of binder dosage on the thermal diffusivity and thermal conductivity is given. The thermal

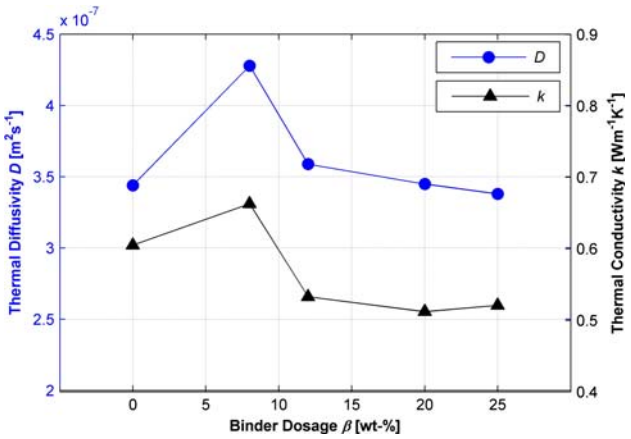

Fig. 6 Measured thermal diffusivities for the pigment tablets with different binder levels

conductivity values are calculated using the tablet densities and the additively calculated heat capacities. When adding binder, the thermal diffusivity gets higher until it reaches a peak at the binder concentration of approximately 8%. The same trend holds for thermal conductivity in this binder concentration range, though the reduced material conductivity of latex means that the values are reduced in relation to those of the diffusivity as latex amount increases. The thermal conductivity is at first increased because the binder fills up the contact void spaces between pigment particles and thus improves the thermal contact (connectivity) of the system. In a recent study, Ridgway and Gane [15] showed that, for a similar pigment, a binder volume fraction of 0.16 of styrene butadiene latex induced a discontinuous rise in viscosity caused by disruptive interaction when the latex particles begin contacting the inter-particle packing of the pigment structure. The same could hold for the pigment-binder system at 8% binder, which is 0.14 in volume fraction (using the densities and solids contents as given in Tables 1 and 2). The addition of binder after the point of contact to the pigment structure causes the pore structure to be disrupted, which will then lower thermal conductivity because of a combination of reduced packing density and the intrinsically less conductive properties of the latex. Porosimetry is now used to clarify these hypotheses.

Porosity and pore structure

Figure 7 shows the pore volume and the pore size distribution of the binder-free tablets, in which the pore size is given as the equivalent capillary diameter omitting the effects of pore shielding. The dispersed binder-free pigment tablet, as would be expected, has distinctly smaller pores compared to the flocculated tablet, but also compared to the dispersed tablets containing binder (Figs. 8 and 9). First of all, it shows that the flocculation of the binder-free coating slurry leads not only to a higher total porosity, but also to larger pores. However, as Fig. 9 shows that the addition of binder also causes a larger average pore size, it confirms that the binder introduces some disruptive interaction to the pigment packing as postulated in the previous section. Laudone et al. [16] examined the shrinkage for coatings of the same pigment binder system. They found that the acrylate binder particles tend to act as rigid balls, at first interfering with the pigment system, which has a rather broad particle size distribution, and then preventing shrinkage by providing resistance to compression forces derived from the retreating meniscus during drying. This observation explains the change in Fig. 9 of the average pore size from 0.1 μm in the binder-free tablet to 0.2 μm for the binder containing tablets. The pore size of 0.2 μm, for the binder-containing tablets, is then in the order of the average binder particle size (compare Table 2), further

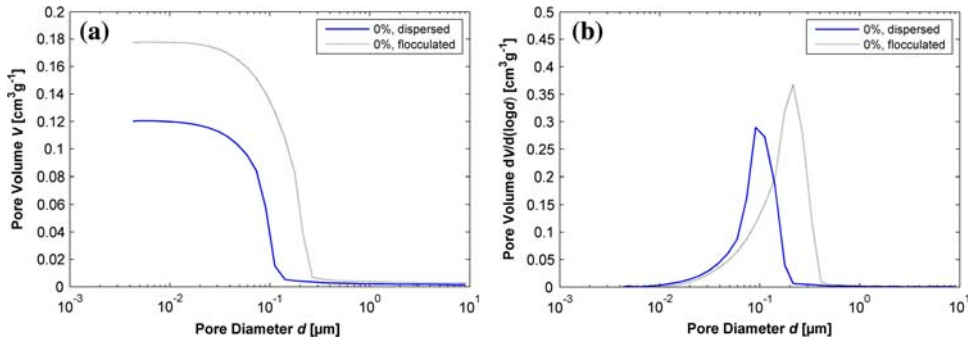

Fig. 7 Cumulative pore volume and pore size distribution for the dispersed and flocculated binder-free tablets

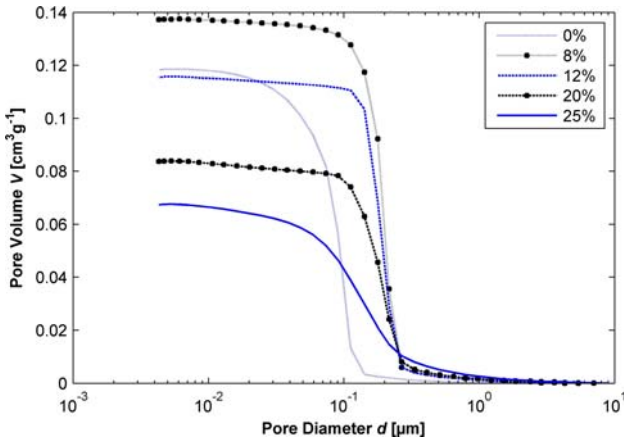

Fig. 8 Cumulative pore volume distribution for the dispersed tablets containing increasing binder dosage

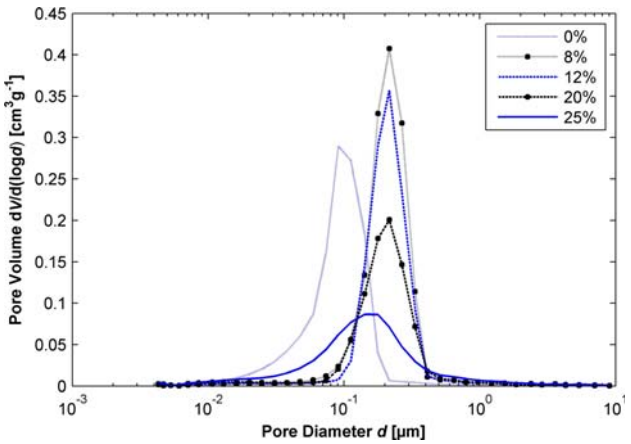

Fig. 9 Pore size distribution for the dispersed tablets containing increasing binder dosage

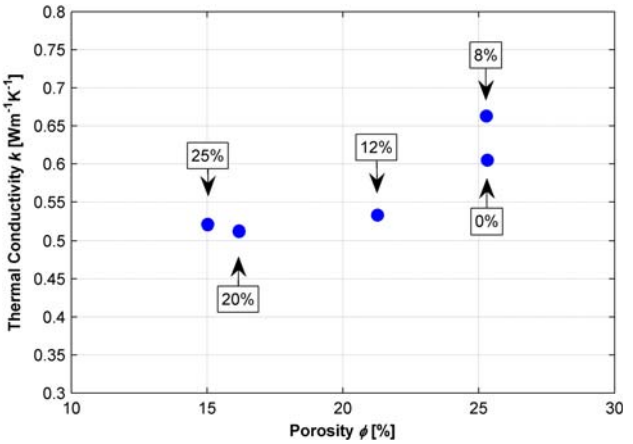

Fig. 10 Thermal conductivity as a function of porosity. The labels indicate the binder dosage in wt%

illustrating the dominant disruptive packing effect of the latex spheres placed amongst the pigment fines.

Modelling

One motivation for the use of the independent structural binder dosage variable c and the pigment variable a in the Modified Lumped Parameter Model is to avoid the use of porosity as the governing parameter. This is, on the one hand, because the term binder dosage is more tangible in terms of coating colour recipes but, on the other hand, even more importantly because porosity alone is not sufficient to describe the thermal behaviour of the system. This can be seen in Fig. 10. Although the tablets of 0 and 8% binder have very similar porosities, the thermal conductivity of the 8% binder-containing tablet is higher than the binder-free tablet. Usually, introducing more binder, which is a material with lower inherent thermal conductivity than the pigment phase, would decrease the total effective thermal conductivity. The fact that, for the same porosity, the modal pore size is changed from 0.1 to 0.2 µm (see Fig. 9) when adding 8% binder shows that the number of pores decreases and, therefore, the connectivity increases. This increased connectivity compensates for the lower inherent thermal conductivity of the binder phase at the binder concentration of 8% so that the effective thermal conductivity increases. When adding more binder, the effective thermal conductivity is lowered due to the increasing influence of the intrinsic more insulating property of the binder.

Translated to the Modified Lumped Parameter Model, this means that the point for the maximum thermal conductivity ($c = 1$) is given for the binder concentration of

8%. For the lower binder concentrations, the connectivity is smaller, and for higher binder concentrations the lower inherent thermal conductivity of the binder, as well as the disruptive interactions of binder particles and pigment, acts to lower the effective thermal conductivity.

This trend is shown in Fig. 11 for the theoretical curves of the Modified Lumped Parameter Model, using pigment size variables of $a = 0.50$, 0.55 and 0.60, compared with the experimental data. The connection of binder dosage and binder variable c was made by using least squares fitting to the theoretical $a = 0.55$ curve, following a multiple linear regression for a quadratic equation:

$$c = x_0 + x_1\beta + x_2\beta^2 \tag{7}$$

where the coefficients are $x_0 = -0.61648$, $x_1 = 1.3567$, $x_2 = 0.95419$.

The mechanisms evoked in this carbonate pigment-binder system differ from the original approach of the model. The talcum system measured by Guérin et al. [14], which was recently analysed using the Modified Lumped Parameter Model [9], showed a very consistent behaviour with the initially constant pigment volume approach, in which the critical pigment volume concentration of the coating was reached at a binder dosage of 20 wt%. The binder variable c was then correlated to the completely filled unit cell of the model ($c = 1$). The lower binder concentrations maintained porous coatings and also porous unit cells in the model, whereas higher binder concentrations showed the increasing influence of the binder with respect to the pigment phase for the coating, the binder filling the voids, which in turn shrank in relation to binder dose in the unit cell of the model.

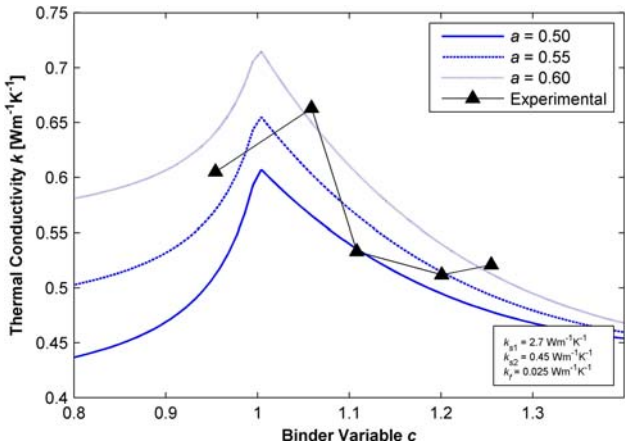

Fig. 11 Theoretical curves of the Modified Lumped Parameter Model and experimental data of thermal conductivity

In this calcium carbonate system, combined with the relatively hard sphere latex, there are several differences that distinguish it from the previously studied talc coating, and the mechanisms of their effective thermal behaviour. The calcium carbonate pigments with a shape factor between one and two (low aspect ratio) are quite blocky compared to the very platy (high aspect ratio) talcum particles. The talc particles, when aligned, pack more densely, with particle thickness being the main controlling parameter, which in talc is rather uniform, compared with the more random packing of the carbonate. This results in a lower pigment variable ($a \approx 0.55$ for the calcium carbonate versus $a \approx 0.8$ for the talcum system) showing that the influence of the pigment material properties is much higher if it is more densely packed. A second difference is the binder used. The styrene butadiene latex used for the talcum system is assumed to be softer and easier film forming than the higher glass transition temperature (T_g) acrylic latex in the calcium carbonate system. The more rigid binder spheres in combination with the blocky particles of the pigment, having its rather broad particle size distribution, increase the tendency for disruptive packing interactions. For that reason the porosities of the calcium carbonate coating are generally quite high, even for the higher binder concentrations. This is in contradiction to the originally proposed three stages approach of unit cells in the model. The unit cells after the point of $c = 1$ are, by definition, non-porous, and this fails to reflect the effect of the (rigid) binder disrupting the pigment packing before it finally fills the remaining voids and becomes non-porous.

The model, therefore, would have to be adapted if one wants to maintain a relation of the model to the practical "thermal porosity", which is defined by the solid phases in

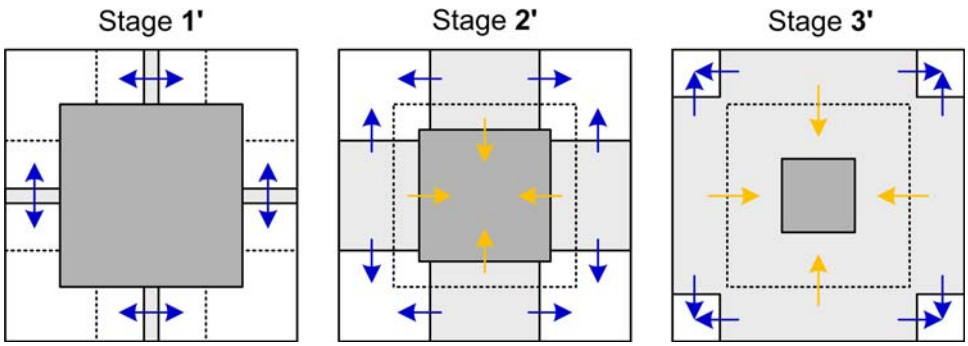

Fig. 12 (*Left* to *right*) Three stages of the unit cell behaviour for the addition of disruptively interacting binder (rigid binder spheres in combination with broad particle size distribution pigment)

the unit cell, and the "structural porosity", which is measured by porosimetry. This can be done by effectively lowering the amount of pigment (see stage 2′ in Fig. 12) in the unit cell when increasing the amount of (disruptive) binder.

Conclusions

In this study, the thermal diffusivity of a calcium carbonate pigment and styrene acrylate binder system was measured by the temperature response of a heated pigment tablet, extending the methodology of Gane et al. [7]. The thermal conductivities were calculated and the pore structures of the tablets were measured using mercury porosimetry. Both thermal diffusivity and thermal conductivity showed a maximum for the binder concentration of 8 wt% based on pigment. Porosimetry confirmed that the initial addition of binder improves connectivity (fewer fine pores at the same total volume) and therefore the thermal properties. Further addition of binder reduces thermal conductivity because of its lower inherent thermal conductivity and its interaction with the pigment packing. The Modified Lumped Parameter Model [9] was used to discuss and illustrate the mechanisms affecting the interconnection of structural and thermal properties. The differences in the structural behaviour of the calcium carbonate coating in this study and a talcum coating reconfirm the importance of coating structures in determining their thermal properties.

Acknowledgements Grateful thanks are given to Omya Development AG for its continuing financial support of this work. A particular thanks also to Dr. Cathy J. Ridgway, Senior Scientist at Omya's R&D Laboratories, Oftringen, Switzerland, for her expertise and support in assisting in the sample construction and determination of coating pore structure.

References

1. Maijala J, Putkisto K, Pietikäinen R, Grön J (2004) Nordic Pulp Paper Res J 19(3):291
2. Kartovaara I, Rajala R, Luukkala M, Sipi K (1985) Conduction of heat in paper, paper making raw materials, Trans 8th fundamental research symposium, Oxford, Mechanical Engineering Publications Ltd, London, pp 381–412
3. Hestmo RH, Lamvik M (2002) J Pulp Paper Sci 28(4):128
4. Crotogino RH (1982) Tappi J, October, pp 97–101
5. Cody HM (2005) Coated paper markets post strong rebound, PaperAge, Mar/Apr, pp 18–19
6. Tsotsas E, Martin H (1987) Chem Eng Process 22:19
7. Gane PAC, Ridgway CJ, Schölkopf J, Bousfield DW (2006) Heat transfer through calcium carbonate-based coating structures: observation and model for a thermal fusing process. Paper presented at the International Printing and Graphic Arts Conference, Cincinnati, Tappi Press
8. Maxwell JC (1873) A treatise on electricity and magnetism. Clarendon Press, Oxford, p 365
9. Gerstner P, Paltakari J, Gane PAC A lumped parameter model for thermal conductivity of paper coatings, Transp. Porous Media (in press). doi:10.1007/s11242-008-9276-y
10. Hsu CT, Cheng P, Wong KW (1995) J Heat Transfer 117:264
11. Landolt-Börnstein, Zahlenwerte und Funktionen, Band IV Technik, 4. Wärmetechnik a, 6. Auflage, Heidelberg, 1980
12. Mark JE (1996) Physical properties of polymers handbook. American Institute of Physics, Woodbury, NY
13. Gane PAC, Kettle JP, Matthews GP, Ridgway CJ (1996) Ind Eng Chem Res 35(5):1753
14. Guérin D, Morin V, Chaussy D, Auriault JL (2001) Thermal conductivity of handsheets, papers and model coating layers, the science of papermaking, 12th fundamental research symposium, Oxford, Fundamental Research Society, Bury, UK, pp 927–945
15. Ridgway CJ, Gane PAC (2007) J Pulp Paper Sci 33(2):71
16. Laudone GM, Matthews GP, Gane PAC (2006) J Colloid Interface Sci 304:180